

## Level structure of $^{103}\text{Ag}$ at high spins

S. Ray<sup>1</sup>, N.S. Pattabiraman<sup>1a</sup>, Krishichayan<sup>1</sup>, A. Chakraborty<sup>1b</sup>, S. Mukhopadhyay<sup>1</sup>, S.S. Ghugre<sup>1</sup>,  
S.N. Chintalapudi<sup>1</sup>, A.K. Sinha<sup>1</sup>, U. Garg<sup>2</sup>, S. Zhu<sup>2,c</sup>, B. Kharraja<sup>2</sup>, and D. Almeded<sup>2</sup>

<sup>1</sup>*UGC-DAE Consortium for Scientific Research,  
Kolkata Centre, Sector III, LB-8,  
Bidhan Nagar, Kolkata 700 098, India;*

<sup>2</sup>*Physics Department, University of Notre Dame,  
Notre Dame IN 46556, USA.*

\*

(Dated: November 1, 2018)

High spin states in  $^{103}\text{Ag}$  were investigated with the Gammasphere array, using the  $^{72}\text{Ge}(^{35}\text{Cl}, 2p2n)^{103}\text{Ag}$  reaction at an incident beam energy of 135 MeV. A  $\Delta J=1$  sequence with predominantly magnetic transitions and two nearly-degenerate  $\Delta J = 1$  doublet bands have been observed. The dipole band shows a decreasing trend in the  $B(M1)$  strength as function of spin, a well established feature of magnetic bands. The nearly-degenerate band structures satisfy the three experimental signatures of chirality in the nuclei; however microscopic calculations are indicative of a magnetic phenomenon.

PACS numbers: 27.60.+j; 23.20.Lv; 23.20.En; 21.10.Tg; 21.10.Ky; 21.60.Ev

### I. INTRODUCTION

Nuclei in the  $A \sim 105$  region with  $Z \sim 50$  and  $N \geq 56$  have low-lying states containing one or more proton holes in the high- $\Omega$   $g_{9/2}$  orbitals, and neutrons in the low- $\Omega$   $g_{7/2}$ ,  $d_{5/2}$  and  $h_{11/2}$  orbitals. These nuclei are also known to be  $\gamma$ -soft (triaxial), with small deformations ( $\beta_2 \sim 0.15$ ) [1, 2, 3, 4]. These conditions are favorable for the observation of (a) magnetic or “shears” band, characterized by a  $\Delta J=1$  sequence, with strong intra-band (M1) transitions, weak crossover (E2) transitions, and decreasing  $B(M1)$  strengths with increasing rotational frequency; and, (b) chiral bands, exhibiting nearly degenerate energy states, with a small, but almost constant, energy difference between the bands. A spontaneous breaking of the chiral symmetry can take place for configurations where the angular momenta of the valence protons, the valence neutrons, and the core are mutually perpendicular. This can occur, for example, when the proton and neutron Fermi levels are located in the lower part of valence proton high-j (particle like) and in the upper part of valence neutron high-j (hole like) subshells, and the core is triaxial.

Recently, P. Dutta *et al.* [5] have reported the possibility of co-existence of the principal and tilted axis rotation in  $^{103}\text{Ag}$ . The possible configuration suggested for these bands was,  $\pi[(g_{9/2})] \otimes \nu[(g_{7/2})(h_{11/2})]$  [5]. Also, in the neighboring nucleus  $^{104}\text{Ag}$ , strong intra-band (M1) transitions have been observed with weak cross over (E2) transitions [1]. These bands were suggested to be based on the  $\pi[(g_{9/2})] \otimes \nu[(g_{7/2})(d_{5/2})(h_{11/2})^2]$  configuration; the deformation parameters  $\beta_2$  and  $\gamma$  were found to be 0.17 and  $29^\circ$ , respectively. Similar configuration involving the degenerate  $(g_{7/2})/(d_{5/2})$  orbitals could give rise to “shears band” in  $^{103}\text{Ag}$  as well.

The first observation of chiral structures in nuclei were reported in  $N = 75$  isotones in the  $A \sim 130$  region. Recently

---

<sup>a</sup>Present address: *Department of Physics, University of York, York YO10 5DD, UK;* <sup>b</sup>Present address: *Department of Physics, Krishnath College, Berhampore 742101, India;* <sup>c</sup>Present address: *Physics Division, Argonne National Laboratory, Argonne IL 60439 USA*

evidence has been presented for a new region of chirality around  $A \sim 104$  [4]. These chiral partners are based on the  $\pi(g_{9/2})^{(-1)} \otimes \nu(h_{11/2})$  configuration. Such configurations are energetically favorable in  $^{103}\text{Ag}$ , hence it is of interest to explore the occurrence of chiral bands (structures) in this nucleus.

Magnetic rotation is expected in weakly deformed nuclei, when high  $j_\pi$  particle of one kind combine with high  $j_\nu$  holes of the other kind of nucleons. Then the vectors  $\mathbf{j}_\pi, \mathbf{j}_\nu$  subtends a large angle with  $\mathbf{J}$  (total angular momentum), specifying the orientation and combining to a large dipole moment. To observe regular bands with many transitions the vectors  $\mathbf{j}_\pi$  and  $\mathbf{j}_\nu$  of the particles and holes should gradually align with  $\mathbf{J}$ . This situation occurs when at least two high  $j$  particles and one high  $-j$  hole form the rotating dipole. In a shell model study of magnetic rotation band, it has been found that regular bands only appear if the core of the nucleus is soft enough such that high  $-j$  particles may induce a slight deformation. The gradual alignment of  $\mathbf{j}_\pi, \mathbf{j}_\nu$  with  $\mathbf{J}$  is reminiscent to the closing of the blades of a pair of shears, leading to the name “shears mechanism”.

This behavior arises naturally in the framework of the tilted axis cranking (TAC) model [6, 7, 8, 9, 10], and has also been described in an intuitive semi-classical approach [11, 12]. In the latter it is found that the interaction between  $\mathbf{j}_\pi$  and  $\mathbf{j}_\nu$  can be described as an effective  $\mathbf{P}_2$  force. The closing of the particle and hole spin vector leads to a specific large drop of  $B(M1)$  values with increasing spin, since  $|\overrightarrow{\mu_\perp}|$  is decreasing with a decreasing opening angle and  $B(M1) \propto |\overrightarrow{\mu_\perp}|^2$ .

The tilted axis cranking (TAC) framework also predicts that in moderately deformed nuclei, the angular momentum is generated from the gradual alignment of spins of quasiparticles (quasineutron or quasiproton) along the direction of total angular momentum. This leads to the violation of signature symmetry due to non-Principal axis rotation which gives rise to regular increase in the M1 transition energies, resulting in tilted axis rotation. We report here on the observation of magnetic rotation, coupled with tilted rotation for three bands in the nucleus  $^{103}\text{Ag}$ .

## II. EXPERIMENT

High-spin states in  $^{103}\text{Ag}$  were populated using the  $^{72}\text{Ge}(^{35}\text{Cl}, 2p2n)^{103}\text{Ag}$  reaction at an incident beam energy of 135 MeV using the ATLAS facility at Argonne National Laboratory. The target was  $1 \text{ mg cm}^{-2}$  thick, evaporated onto a  $15 \text{ mg cm}^{-2}$ -thick gold foil. A thin ( $40 \mu\text{g cm}^{-2}$ ) Al layer was evaporated between the target and the backing to avoid migration of the target material into the gold. De-exciting  $\gamma$  rays were detected with the Gammasphere detector array in its “stand alone” mode; the array comprised of 101 Compton-suppressed Ge detectors at the time of the experiment. Events were recorded when at least three suppressed Ge detectors in the array detected  $\gamma$  rays within the prompt coincidence time window. The total coincidence data set consisted of approximately  $2 \times 10^9$  “triple coincidence” events. Data were sorted into the conventional  $(E_\gamma)^N$  ( $N=3,4$ ) histograms and were analyzed using RADWARE [13] and IUCSORT [14, 15, 16] software.

## III. RESULTS

### A. Level Scheme

The partial level scheme for  $^{103}\text{Ag}$  obtained from this experiment is shown in Fig. 1. Multipolarity of the de-exciting  $\gamma$ -rays of  $^{103}\text{Ag}$  were deduced from the  $\gamma$ -ray coincidences and angular correlations [17, 18]. The higher fold coincidence data were unfolded into doubles and were sorted into the conventional angle-dependent matrices. Two dimensional histograms were generated for events where one of the  $\gamma$ -transition was detected in the  $90^\circ$  ring while its coincidence partner was detected at  $31.7^\circ$  or  $37.3^\circ$ .

The data from these two rings were summed up for better statistics, and the average angle of  $35^\circ$  is used in the subsequent text. Another matrix was similarly created with coincidence data between the  $90^\circ$  and  $145^\circ$  detectors ( $145^\circ$  is the average angle for the detectors at  $142.6^\circ$  or  $148.3^\circ$  ring).

In our procedure, we define the intensity asymmetry ratio  $R_{int}$  as

$$R_{int} = \frac{I_{\gamma_1} \text{ at } 35^\circ \text{ and } 145^\circ; \text{ gated with } \gamma_2 \text{ at } 90^\circ}{I_{\gamma_1} \text{ at } 90^\circ; \text{ gated with } \gamma_2 \text{ at } 35^\circ \text{ and } 145^\circ}$$

Assuming stretched transitions, the  $R_{int}$  value is  $\sim 0.9$  for quadrupoles and  $\sim 0.55$  for dipoles when gated on an  $E(2)$  transition. When the gating transition was a dipole the corresponding values were  $R_{int} \sim 1.7$  for quadrupole and  $\sim 0.9$  for dipoles. These ratios can be used to make reliable spin assignments by comparing the present results with those of  $\gamma$  rays belonging to  $^{103}\text{Ag}$  and its neighboring nuclei whose multipolarity has been established previously.

The presence of cross-over transitions (when observed) corroborated these assignments. Representative values of  $R_{int}$  are listed in Table I and plotted as a function of  $\gamma$ -ray energy in Fig. 2.

Overall, the level scheme is in good agreement with the most recent work [5] but has been considerably extended, with the addition of more than 60 new transitions. The level sequences of interest are labeled as Band A, Band B and Band C; Fig. 3 shows the gated coincidence spectra for Bands C and A.

Band A has been observed for the first time and consists of a sequence of  $\Delta J=1$  transitions of energy(multipolarity) 428(M1), 402(M1), 488(M1), 504(M1), 513(M1), 570(M1), 830(E2), respectively (all energies are listed in keV in this paper). The 1225(M1), 1272(M1) and 1338(M1) transitions connect this band with Band B which has been extended with the observation of the following new transitions: 502, 529(M1), 697(M1), 1045(E2) and 1226(E2).

The 1225-, 1338- and the 1272-keV transitions connect the newly observed Band A with Band B. Their M1 assignment may be argued as follows: Let us assume all these connecting transitions are E1's. For an E1 1225-keV transition the multiplicities of the transitions which de-excite from the 6166.7-keV level would be 402(M1) and 830(E2). This would result in a substantial intensity difference (typically about 5 orders of magnitude) between the 830(E2) and the 1225-keV(E1) transition. However, experimentally they are found to have nearly the same intensities. Thus, the 1225-keV transition cannot be assigned an E1 multipolarity.

If the 1338-keV transition were an E1, this would imply an E1 also for the 402-keV ( $\Delta J = 1$ ) transition and an M2 multipolarity for the cross-over 830-keV transition, which is not favored by lifetime arguments. Similar arguments hold true for the 1272-keV transition as well.

When gated by a sum gate of 235-and 309-keV ( $\Delta J = 1$ ) M1 transitions, we obtained an  $R_{int}$  value of 0.67 for the 1272-keV transition. These gates are free from any contamination from neighboring nuclei. Thus the 1272-keV transition involves a  $\Delta J = 1$  change in angular momentum. The average  $R_{int}$  value of known M1 transitions using the same gate was  $\sim 0.7$ . Similar values were obtained for established M1 transitions in the neighboring nuclei. Further, using the same gate a value of  $\sim 0.9$  was obtained for established E1 transitions. Similar values have been obtained for E1 transitions in the neighboring  $^{104}\text{Ag}$  nucleus, also. Hence the 1272-keV transition is tentatively assigned as an M1 transition and the band-head for the Band B is assigned  $J^\pi = 27/2^-$ .

We have observed a weak crossover transition of 830-keV (whose multipolarity could not be determined) for the lowest two members of the band. However, the 402-and 428-keV transitions have  $\Delta J = 1$ ; these are assigned M1 multipolarity. The  $J^\pi=29/2^-$  assignment is further corroborated by the observation of an M1 transition of 1338 keV ( $29/2_A^- \rightarrow 27/2_B^-$  where the subscript denotes the corresponding band). The present statistics did not permit us to assign the multipolarity for the 570-keV transition; all in-band transitions have been assigned M1 multipolarity, however, based on the results for the more intense transitions in the lower part of the band.

Band B was known up to  $J^\pi = 29/2^-$  and  $E_x = 5470.7$  keV [5]. The present investigation has identified five new members belonging to this band: 502(M1), 529(M1), 697(M1), 1045(E2) and 1226-keV(E2). The angular correlation procedure employed in this work successfully reproduced the multipolarity of the previously-reported transitions. The coincidence relations indicated that 1226- and 1045-keV were crossover transitions and the corresponding  $\Delta J = 1$  transitions are of 516, 529 and 697 keV. The  $R_{int}$  values indicated that the 529-keV and 697-keV transitions are indeed  $\Delta J = 1$ . We could not deduce the multipolarity for the 1045- and 1226-keV transitions due to the presence of  $\gamma$ -rays of similar energy, in yrast and other non-yrast bands of  $^{103}\text{Ag}$ . However, the occurrence of M1 transitions (516 keV and 529 keV) helped us assign an E2 nature to the 1045 keV crossover transition and, on similar basis, the 1226-keV [529-keV (M1) + 697-keV (M1)] transition has also been assigned an E2 multipolarity.

The sequence labeled as Band C has been observed for the first time. The in-band members of this sequence are 181(M1), 282(M1), 289(M1), 359(M1), 369(M1), 383(M1), 432(M1), 433(M1) 543(M1), 1570(E1) and 1748(E1). We have also observed two crossover transitions of 801(E2) and 815 keV(E2). Band C is linked to Band B with 635(M1), 695(M1), 870(E2) and 1002(E2) transitions, the multiplicities of which establish the negative parity of this band. The present statistics permitted us to assign  $\Delta J = 1$  for the 695-keV transition. Further, both the 695- and 1002-keV transitions originate from the same level and connect to levels differing in spin by one unit. The possibilities for the electromagnetic character for these two transitions are, then, M1 and E2 or E1 and M2, respectively. The E1 and M2 combination is not likely because, these transitions would then have lifetimes that are different by almost six orders in magnitude. This is inconsistent with the experimental observations as both the transitions de-excite from the same level, and are observed in prompt coincidence with their respective coincidence  $\gamma$ -transitions. Hence, the transitions have been assigned M1 and E2 multiplicities, respectively, and the de-exciting level is tentatively assigned as  $J^\pi=(25/2^-)$ . A similar situation prevails for the 635- and 870-keV transitions, so the corresponding de-exciting level is tentatively assigned  $J^\pi=(23/2^-)$ .

The present statistics did not permit us to undertake the multipolarity assignments for weak 1570- and 1748-keV inter-band transitions.

## B. DSAM Analysis

As mentioned above, Bands A, B and C, have very intriguing properties : (a) Band-A exhibits characteristics of magnetic rotation, a phenomena reported in the neighboring nuclei; and (b) Band-B and Band-C ( $\Delta J=1$ , rotational band doublets) show experimental fingerprints of chiral-partners. These are discussed in detail in the subsequent sections. To further explore the nature of the bands, we have performed DSAM analysis of the various transitions in these bands.

The target thickness (1 mg  $cm^{-2}$  thick, evaporated onto a 15 mg  $cm^{-2}$ - thick gold foil) provided sufficient stopping power to slow down and stop the recoiling nuclei and to allow DSAM lifetime measurements to be performed. Angle-dependent matrices were formed such that one of the matrices had coincidence events from detectors at  $31.7^\circ$ ,  $37.4^\circ$  (average  $\sim 35^\circ$ ) versus detectors at  $90^\circ$ , and another had events from detectors at  $142.6^\circ$ ,  $148.3^\circ$  (average  $\sim 145^\circ$ ) versus detectors at  $90^\circ$ .

Background subtracted spectra were generated by gating on the  $90^\circ$  detectors. Transitions that exhibited Doppler broadened line shapes were fitted using the Lineshape code of Wells and Johnson [19] from which lifetimes and the corresponding transition strengths have been obtained.

The Lineshape analysis code was used to generate 5000 Monte Carlo simulations for the velocity history of recoiling nuclei traversing through the target and backing material in time steps of 0.001 ps. Electronic stopping powers were taken from the shell-corrected tabulations of Northcliff and Shilling [20].

The major source of systematic errors in DSAM lifetime measurements are related to

1. The uncertainties due to the stopping power parameterization adopted to describe the slowing down process of the recoiling ions.
2. The prescription followed for the feeding of the band levels from unobserved transitions *viz.* the side feeding.

Other uncertainties would include systematic errors due to the parameterization of the background, and instrumental errors, if any. However the contribution from these is not expected to be significant.

In the present work information on the slowing down was carried out using the prescription of Northcliff and Shilling and were repeated using the electronic stopping powers of Zeigler [21]. The lifetime values so obtained are similar, within error limits. This value provided us with the typical uncertainties due to parameterization of stopping power.

The present data has been analyzed using top-gates when possible which eliminates the uncertainties from side-feeding. These values have been used to cross-check the value when gated from below, thus minimizing the systematic errors due to side-feeding.

The uncertainties in lifetimes from the fits were determined by a statistical method using the subroutine MINOS[22] by varying the parameters until the  $\chi^2$  reaches the lowest value,  $\chi_{min}^2$ ; this point determines the best-fit parameter values. The region over which  $\chi^2$  takes on a value between  $\chi_{min}^2$  and  $\chi_{min}^2+1$  corresponds to ‘‘one standard deviation’’ or 68% confidence interval. The uncertainty for a given parameter was found by varying that parameter in steps above (below) its best value. At each step, this parameter was fixed and  $\chi^2$  was re-minimized by varying all other parameters. The step at which the re-minimized  $\chi^2$  equaled  $\chi_{min}^2+1$  was used for positive (negative) uncertainty for this parameter.

Doppler-broadened lineshapes were clearly observed for all levels above  $J^\pi=27/2^-$  in Band B and Band C, and for the levels above  $J^\pi=29/2^-$  in Band A. Representative line-shape fits are depicted in Fig. 4.

For each band, B(M1) and B(E2) transition rates have been extracted using the equations given in [23]. The measured lifetimes along with the corresponding B(M1) and B(E2) values are enumerated in Table II where the values correspond to the calculations following the Northcliff and Shilling prescription. In calculating the B(M1) values, a mixing ratio  $\delta=0$  was assumed for all  $\Delta J=1$  transitions.

## IV. DISCUSSION

As pointed out earlier, Band A resembles a magnetic band, where as Bands B and C exhibit the experimental fingerprints of chiral-partners. A number of nearly-degenerate  $\Delta J = 1$  bands have been observed in the past few years in the  $A \sim 130$  (see, for example, Refs. [24, 25, 26, 27]) and  $A \sim 100$  [4, 28, 29, 30, 31] regions, and have been proposed as chiral partners. The main fingerprints of chirality have been identified [4] as:

- (a) Energy degeneracy between doublet bands;
- (b) a constant  $S(I)$  parameter, defined as  $S(I) = [E(I) - E(I - 1)]/2I$ , as a function of spin; and,
- (c) staggering of  $B(M1)/B(E2)$  values.

In Fig. 5, we plot these three fingerprints for Bands B and C, and they appear to satisfy all of the aforementioned criteria. For example, in Fig. 5(a), the excitation energies of the bands are shown as a function of spin. Where it can be seen that, the energy separation between states of the same spin decreases gradually with increasing spin,

eventually becoming nearly degenerate ( $\Delta E = 19$  keV) at spin  $33/2^-$ . Such a behavior is characteristic of the “chiral” bands observed so far and has been attributed to a gradual transition from planar tilted rotation to aplanar tilted rotation. At spins above  $J = 31/2\hbar$ , it is expected that both the bands remain close to degenerate in energy.

The second characteristic, which essentially serves as a consistency check, is the independence of  $S(I) = [E(I) - E(I - 1)]/2I$  as a function of spin  $I$ . As seen from Fig. 5(b),  $S(I)$  is generally independent of the spin  $I$ . In Fig. 5(c), the  $B(M1)/B(E2)$  ratios indicate a certain staggering as a function of spin. These observations are very similar to those reported for  $^{104}\text{Rh}$  [4], and  $^{100}\text{Tc}$  [28], where the corresponding bands have been identified as chiral doublets.

Traditionally, magnetic and chiral bands have been well understood within the frame work of TAC. In addition, the semi-classical approach of Machiavelli *et al.* [11, 12] provides a qualitative understanding of the phenomenon of magnetic rotation. We have applied both these approaches in order to understand the observed level structure.

Self-consistent cranking model calculations were performed for comparison with Band A, B and C. Three-dimensional tilted axis cranking (3D TAC) calculations were, then, carried out using the same set of parameters to investigate the possible existence of magnetic and chiral rotation in  $^{103}\text{Ag}$ . For the three  $\Delta J=1$  bands, we found  $\theta < 90^\circ$ , which is in accordance with their  $\Delta J=1$  character. The deformation parameters,  $\epsilon$  and  $\gamma$ , and the tilt angle  $\theta$  and  $\phi$  were obtained for a given frequency  $\hbar\omega$  and for a particular configuration, then searching for a local minimum on the multi parameter surface of the total routhian. All the calculations done below find a minimum with  $\phi = 0$  which corresponds to planar TAC solution. The proton and neutron Fermi surfaces lie too far from the  $N = 50$ ,  $Z = 50$  closed shell to warrant using a quasiparticle treatment of the protons and neutrons. The gap parameter  $\Delta$  was chosen as 80% of the odd-even mass difference  $\Delta_{oe}$  for protons and neutrons. The proton and neutron chemical potentials,  $\lambda_\pi$  and  $\lambda_\nu$ , were chosen such that the particle number of  $Z \sim 47$  and  $N \sim 56$  could be reproduced.

### A. Band A

Band A exhibits characteristics of magnetic rotation, a phenomenon already well established in the neighboring nuclei [1]. As mentioned in Ref. [11], the shears mechanism is generated by the residual interaction between the proton and the neutron blades with a strength proportional to  $P_2(\cos\theta)$ , where  $\theta$  is the shears angle.

Experimentally, the shears angle for a pure shears band can be estimated at each observed spin  $J$ , by calculating  $\theta = \cos^{-1}[(J^2 - j_\pi^2 - j_\nu^2)/2j_\pi j_\nu]$ . The excitation energy for each state for pure shears should result solely from the closing of blades.

Assuming a pure shears band (with no contribution from the core), the energies of the states in this band relative to the  $J^\pi = 27/2^-$  level were calculated by using the  $\pi(g_{9/2}) \otimes \nu(h_{11/2})(g_{7/2})$  configuration. The highest experimentally observed spin for this sequence is  $J = 39/2$ . The energies,  $V(\theta)$  are plotted as a function of  $\theta$  in the form  $V(\theta) = \frac{1}{2}V_2(3\cos^2\theta - 1) + V_0$ , which is appropriate for a force generated by the exchange of a quadrupole phonon in Fig. 6. From these results, the strength of the interaction was obtained to be  $318 \pm 40$  keV, which is typical for such bands in this region.

In Fig. 7, the aligned angular momentum  $i_x$  of Band A has been plotted as a function of rotational frequency  $\omega$ . The reference parameters for  $i_x$  were:  $\mathfrak{S}_0 = 7.0\hbar^2/\text{MeV}$  and  $\mathfrak{S}_1 = 15.0\hbar^4/\text{MeV}^3$  [32]. The aligned angular momentum plot shows an up bend of  $4\hbar$  which continues with increasing  $\hbar\omega$ .

The TAC calculation for Band A were performed assuming the  $\pi(g_{9/2})^3 \otimes \nu g_{7/2} h_{11/2}$  five quasiparticle configuration. The equilibrium value for the deformation parameter is found to be  $\epsilon \sim 0.10$  with a decreasing trend along the band. The value of  $\gamma$  is found to be  $19^\circ$  and increases along the band. The observed spin, energy, and  $B(M1)$  values of Band A are plotted in Fig. 8 together with the results from the TAC calculation [8, 10]. The calculated  $E(I)$  plot is shown by the dashed line whereas the experimental data is represented as a solid line. There is a reasonable agreement between the experimental values and TAC calculation for both the energy and the transition rates. The experimental  $I(\omega)$  plot (Fig. 8) show signs of single particle alignment that is not reproduced in the calculation. The fact that the  $\Delta J = 2$ , E2 transitions are very weak in the experiment can also be understood from the calculations where the  $B(E2)$  rates are predicted to be close to zero.

The  $\mathfrak{S}_2/B(E2)$  ratio for Band A is  $\sim 450 \hbar^2 \text{MeV}^{-1} (eb)^{-2}$ , which is comparable to that of a magnetic rotor. This again indicates that Band A in  $^{103}\text{Ag}$  arises due to magnetic rotation. The vital fingerprint of the shears mechanism is the characteristic drop in the magnitude of  $B(M1)$  with increasing rotational frequency because of the rapid closure of shears. The experimental  $B(M1)$ 's are presented in Table II. The typical values of  $B(M1)$  are  $\sim 3-5 \mu_N^2$ , with a decreasing tendency with spin, a signature of magnetic-rotational bands [33].

## B. Bands B and C

Although Band B and C show experimental fingerprints of chiral-partners, the tilted axis cranking calculations for these bands yielded a planar solution ( $\phi = 0$ ), essentially ruling out chiral behavior. Both these bands are governed by  $g_{9/2}$  proton orbital and  $g_{7/2}/d_{5/2}$ ,  $h_{11/2}$  neutron orbitals where as Band C has a different  $g_{7/2}/d_{5/2}$  neutron configuration relative to Band B. The small deformation ( $\epsilon_2 \sim 0.13$ ) leads to planar tilted solution with  $\gamma \sim 15^\circ$ . Figs. 9,10 show that the experimental energies and the spins of the bands agree with the calculated values. While the transition rates, B(M1), of Band B are very well reproduced by the calculation, the large B(M1) seen in Band C can not be fully understood. The calculated B(E2)'s of Band B and C are considerably larger than those in Band A, which would explain why there are substantial E2 transitions in Bands B and C but not in Band A. Bands B and C show some of the characteristics of a magnetic band and also have some of the characteristics of a tilted rotational band.

As mentioned earlier, it is tempting to assign Bands B and C as chiral partners, based on the experimental signatures. However, the tilted axis cranking calculation does not support this interpretation. Instead, the calculation indicates that the two bands are build on different quasi-particle configurations. The similar characteristics exhibited by these two bands may be due to high level density at the neutron Fermi surface, resulting in several configurations with similar properties. Combined with the high degree of symmetry breaking in the mean field solution, this can lead to mixing of different quasiparticle configurations which will be manifested in the experimental results as an irregular band structure, as for Bands B and C.

For Band B, the aligned angular momentum shows an initial jump of  $2\hbar$  (see Fig. 7) after which it remains constant at  $8\hbar$ . For Band C, at a rotational frequency of approximately  $0.35 \text{ MeV}/\hbar$  (as shown in Fig. 7) the aligned angular momentum curve shows a rapid decrease in rotational frequency and an increase of approximately  $3\hbar$  in aligned angular momentum. This effect can be caused by mixing of different configurations or by a partial alignment of the  $[(g_{7/2})/(d_{5/2})]$  neutron.

The  $\mathfrak{S}_2/B(E2)$  ratio for Bands B and C is  $\sim 250 \hbar^2 \text{MeV}^{-1} (eb)^{-2}$ . The absence of the aplanar solution and the large  $\mathfrak{S}_2/B(E2)$  are supportive of a magnetic rotation for the Bands B and C, even though they qualitatively resemble chiral partners. The smaller value of  $\mathfrak{S}_2/B(E2)$  and larger deformation of Band B and C relative to Band A indicate that these bands have a larger component of collective rotation relative to the pure magnetic rotation of Band A. As pointed out earlier this is also supported by the presence of several E2 transitions in Band B and C. The semi classical formalism does not work for these bands, also pointing to the presence of phenomena other than magnetic rotation.

With the high level density at the neutron Fermi surface in  $^{103}\text{Ag}$ , there might be bands with different configurations manifesting very similar properties in accordance with the chiral fingerprints. Further investigations, both in theory and experiment, to explore these issues would clearly be useful.

## V. CONCLUSIONS

The level structure of  $^{103}\text{Ag}$  has been substantially extended up to  $E_x = 8240 \text{ keV}$  and  $J^\pi = 39/2^-$  with the observation of more than 60 new transitions. We have observed an intriguing structure in this nucleus, *viz.* two bands that qualitatively exhibit all the experimental fingerprints of chiral partners, but do not correspond to an aplanar tilted axis cranking solution. Also these bands reveal a larger collective rotational component than that in the well-established pure magnetic rotational bands. The  $\Delta J=1$  sequence (Band A) resembles a magnetic rotational band. The lifetimes of the states in this band qualitatively follow the established trend for shears bands. An interaction strength of  $318 \pm (40) \text{ keV}$  has been obtained using the semi-classical formalism of Macchiavelli *et al.* [11, 12].

## VI. ACKNOWLEDGMENTS

We gratefully acknowledge illuminating discussions with Prof. S. Frauendorf and Dr. R. V. F. Janssens. We also thank Prof. J. C. Wells and Mr. P. Dutta for their help with the computer code LINESHAPE and the ATLAS scientific staff for help with the Gammasphere experiment. This work has been supported in part by the INDO-US, DST-NSF grant (DST-NSF/RPO-017/98), by the U.S. National Science Foundation under grants no. INT-01115336

and PHY04-57120, and the University of Notre Dame.

- 
- [1] P. Datta *et al.*, Phys. Rev. C **69**, 0441317 (2004).
  - [2] A. Gadea *et al.*, Phys. Rev. C **55**, R1 (1997).
  - [3] D. J. Jenkins *et al.*, Phys. Rev. Lett. **83**, 500 (1999).
  - [4] C. Vaman, D.B. Fossan, T. Koike, K. Starosta, I.Y. Lee, A.O. Macchiavelli, Phys. Rev. Lett. **92**, 032501 (2004).
  - [5] P. Datta *et al.*, Phys. Rev. C **67**, 014325 (2003).
  - [6] S. Frauendorf, Nucl. Phys. **A557**, 259c (1993).
  - [7] S. Frauendorf, Z. Phys. A **358**, 163 (1997).
  - [8] S. Frauendorf, Nucl. Phys. **A677**, 115 (2000).
  - [9] V.I. Dimitrov, S. Frauendorf, F. Dönau, Phys. Rev. Lett. **84**, 5732 (2000).
  - [10] V.I. Dimitrov, F. Dönau, S. Frauendorf, Phys. Rev. C **62**, 024315 (2000).
  - [11] A.O. Macchiavelli, R.M. Clark, P. Fallon, M.A. Deleplanque, R.M. Diamond, R. Krucken, I.Y. Lee, F.S. Stephens, S. Asztalos, K. Vetter, Phys. Rev. C **57**, R1073 (1998).
  - [12] A.O. Macchiavelli, R.M. Clark, M.A. Deleplanque, R.M. Diamond, P. Fallon, I.Y. Lee, F.S. Stephens, K. Vetter, Phys. Rev. C **58**, R621 (1998).
  - [13] D.C. Radford, Nucl. Instr. Methods Phys. Res. A **361**, 297 (1995).
  - [14] N.S. Pattabiraman, S.N. Chintalapudi and S.S. Ghugre, Nucl. Instrum. Methods Phys. Res. A **526**, 432 (2004).
  - [15] N.S. Pattabiraman, S.N. Chintalapudi and S.S. Ghugre, Nucl. Instrum. Methods Phys. Res. A **526**, 439 (2004).
  - [16] N.S. Pattabiraman, S.S. Ghugre, S.K. Basu, U. Garg, S. Ray, A.K. Sinha, S. Zhu, Nucl. Instrum. Methods Phys. Res. A **562**, 222 (2006).
  - [17] F.S. Stephens, M.A. Deleplanque, R.M. Diamond, A.O. Macchiavelli, J.E. Draper, Phys. Rev. Lett. **54**, 2584 (1985).
  - [18] C.W. Beausang, D. Prevost, M.H. Bergstrom, G. de France, B. Haas, J.C. Lisle, Ch. Theisen, J. Timar, P.J. Twin, J.N. Wilson, Nucl. Instrum. Methods Phys. Res. A **364**, 560 (1995).
  - [19] J.C. Wells and N.R. Jhonson, Report No. **ORNL-6689**, 44 (1991).
  - [20] L.C. Northcliffe, R.F. Schilling, Nucl. Data Tables A **7**, 233 (1970).
  - [21] J.F. Zeigler, J.E. Beirsack and U. Littmark, The Stopping Power and Ranges of Ions in Matter (Pergamon, New York, 1985) Vol. **I**, software SRIM2000.
  - [22] F. James and M. Roos, Comput. Phys. Commun. **10**, 343 (1975).
  - [23] C.J. Chiara *et al.*, Phys. Rev. C **64**, 054314 (2001).
  - [24] S. Zhu *et al.*, Phys. Rev. Lett. **91**, 132501 (2003).
  - [25] G. Rainovski *et al.*, Phys. Rev. C **68**, 024318 (2003).
  - [26] K. Starosta, C.J. Chiara, D.B. Fossan, T. Koike, T.T.S. Kuo, D.R. LaFosse, S.G. Rohozinski, Ch. Droste, T. Morek, J. Srebrny, Phys. Rev. C **65**, 044328 (2002).
  - [27] K. Starosta, T. Koike, C.J. Chiara, D.B. Fossan, D.R. LaFosse, Nucl. Phys. **A 682**, 375c (2001).
  - [28] P. Joshi *et al.*, Eur. Phys. J. A **24**, 23 (2005).
  - [29] P. Joshi *et al.*, Phys. Lett. B **595**, 135 (2004).
  - [30] J. Timar *et al.*, Phys. Lett. B **598**, 178 (2004).
  - [31] P. Joshi *et al.*, Phys. Rev. Lett. **98**, 102501 (2007).
  - [32] P.H. Regan *et al.*, Nucl. Phys. **A586**, 351 (1995).
  - [33] S. Frauendorf, Rev. Mod. Phys. **73**, 463 (2001).

TABLE I: Gamma transition energy ( $E_\gamma$ ) in keV, Excitation energy ( $E_x$ ) in keV, initial and final spins for the transition,  $R_{int}$ , and multipolarity for the states in  $^{103}\text{Ag}$ .

$E_\gamma$	$E_x$	$J_i^\pi \rightarrow J_f^\pi$	$I_\gamma[1][2]$	$R_{int}[3][4]$	Multipolarity
69.9	3104.0	$19/2^- \rightarrow (17/2^-)$	10.0(10)		(M1)
180.8	3402.2	$(19/2^-) \rightarrow (17/2^-)$	3.4(3)		(M1)
234.9	3338.9	$21/2^- \rightarrow 19/2^-$	36.8(40)	0.57(6) <sup>q</sup>	M1
252.5	3104.0	$19/2^- \rightarrow 17/2^-$	2.8(3)	0.55(6) <sup>q</sup>	M1
260.0	833.7	$13/2^+ \rightarrow 11/2^+$	100(10)	1.0(1) <sup>d</sup>	M1
282.3	3973.9	$(23/2^-) \rightarrow (21/2^-)$	3.4(3)	0.48(6) <sup>q</sup>	(M1)
289.4	3691.0	$(21/2^-) \rightarrow (19/2^-)$	3.8(4)	0.42(6) <sup>q</sup>	(M1)
296.6	2851.5	$(17/2^-) \rightarrow (15/2^-)$	10.0(10)		(M1)
309.0	3647.9	$23/2^- \rightarrow 21/2^-$	34.2(40)	0.57(6) <sup>q</sup>	M1
330.5	1803.7	$17/2^+ \rightarrow 15/2^+$	63.7(70)	0.62(8) <sup>q</sup>	M1
358.8	3402.2	$(19/2^-) \rightarrow (17/2^-)$	1.3(1)		(M1)
361.9	4426.0	$27/2^- \rightarrow 25/2^-$	23.8(20)	0.53(6) <sup>q</sup>	M1
368.8	4340.8	$(25/2^-) \rightarrow (23/2^-)$	2.3(2)	0.55(6) <sup>q</sup>	(M1)
382.9	5157.0	$(29/2^-) \rightarrow (27/2^-)$	1.79(20)	0.72(10) <sup>d</sup>	(M1)
402.4	6166.7	$(31/2^-) \rightarrow (29/2^-)$	3.7(4)	0.44(6) <sup>q</sup>	(M1)
416.2	4064.1	$25/2^- \rightarrow 23/2^-$	31.3(30)	0.67(8) <sup>q</sup>	M1
427.8	5764.3	$(29/2^-) \rightarrow (27/2^-)$	0.50(6)		(M1)
432.2	4774.9	$(27/2^-) \rightarrow (25/2^-)$	1.6(1)	0.44(6) <sup>q</sup>	(M1)
433.2	5591.0	$(31/2^-) \rightarrow (29/2^-)$	0.87(8)	0.50(6) <sup>q</sup>	(M1)
487.5	6654.0	$(33/2^-) \rightarrow (31/2^-)$	1.6(2)	0.42(6) <sup>q</sup>	(M1)
502.0	6669.7	$\rightarrow (33/2^-)$	$W^2$		
503.6	7157.8	$(35/2^-) \rightarrow (33/2^-)$	1.5(2)	0.45(6) <sup>q</sup>	(M1)
512.6	7670.4	$(37/2^-) \rightarrow (35/2^-)$	1.4(2)	0.43(6) <sup>q</sup>	(M1)
515.6	4941.6	$29/2^- \rightarrow 27/2^-$	24.0(20)	0.77(7) <sup>d</sup>	M1
529.1	5470.7	$(31/2^-) \rightarrow 29/2^-$	3.42(40)	0.55(6) <sup>q</sup>	(M1)
542.8	6133.8	$(33/2^-) \rightarrow (31/2^-)$	0.70(1)	0.54(6) <sup>q</sup>	(M1)
549.1	3104.0	$19/2^- \rightarrow (15/2^-)$	2.2(1)		(E2)
563.7	573.7	$11/2^+ \rightarrow 9/2^+$	200.0	0.69(7) <sup>q</sup>	M1
569.9	8240.3	$(39/2^-) \rightarrow (37/2^-)$	0.30(5)		(M1)
635.0	3973.9	$(23/2^-) \rightarrow 21/2^-$	0.18(1)		(M1)
639.5	1473.2	$15/2^+ \rightarrow 13/2^+$	100(10)	0.75(10) <sup>q</sup>	M1
694.8	4342.7	$(25/2^-) \rightarrow 23/2^-$	1.45(20)	1.30(15) <sup>d</sup>	(M1)
697.0	6167.7	$(33/2^-) \rightarrow (31/2^-)$	4.1(4)	0.69(8) <sup>q</sup>	(M1)
725.2	4064.1	$25/2^- \rightarrow 21/2^-$	3.6(4)	0.82(9) <sup>q</sup>	E2
778.1	4426.0	$27/2^- \rightarrow 23/2^-$	8.7(8)	0.95(6) <sup>q</sup>	E2
801.0	4774.9	$(27/2^-) \rightarrow (23/2^-)$	0.50(1)	2.20(23) <sup>d</sup>	(E2)
815.1	5157.0	$(29/2^-) \rightarrow (25/2^-)$	0.31(1)		(E2)
823.7	833.7	$13/2^+ \rightarrow 9/2^+$	100(10)	0.89(10) <sup>q</sup>	E2
830.2	6166.7	$(31/2^-) \rightarrow (27/2^-)$	0.20(2)		(E2)
869.9	3973.9	$(23/2^-) \rightarrow 19/2^-$	1.58(20)		(E2)
877.5	4941.6	$(29/2^-) \rightarrow 25/2^-$	5.5(5)	2.70(31) <sup>d</sup>	(E2)
892.0	3034.1	$(17/2^-) \rightarrow (15/2^-)$	3.9(4)		(M1)
899.5	1473.2	$15/2^+ \rightarrow 11/2^+$	100(10)	1.50(11) <sup>d</sup>	E2
970.0	1803.7	$17/2^+ \rightarrow 13/2^+$	100(10)	1.03(12) <sup>q</sup>	E2
1001.9	4340.8	$(25/2^-) \rightarrow 21/2^-$	0.80(1)		(E2)
1044.7	5470.7	$(31/2^-) \rightarrow 27/2^-$	2.5(3)	1.76(13) <sup>d</sup>	(E2)
1225.1	6166.7	$(31/2^-) \rightarrow (29/2^-)$	0.60(6)		(M1)
1226.1	6167.7	$(33/2^-) \rightarrow (29/2^-)$	2.8(3)		(E2)
1272.4	5336.5	$(27/2^-) \rightarrow 25/2^-$	0.80(1)	0.67(10) <sup>d</sup>	(M1)
1300.3	3104.0	$19/2^- \rightarrow 17/2^+$	38.1(30)	0.84(13) <sup>d</sup>	E1
1308.4	2142.1	$(15/2^-) \rightarrow 13/2^+$	1.1(1)	0.43(8) <sup>q</sup>	(E1)
1338.3	6166.7	$(29/2^-) \rightarrow 27/2^-$	2.7(3)	0.59(5) <sup>d</sup>	(M1)
1378.3	2851.5	$17/2^- \rightarrow 15/2^+$	11.9(10)	0.96(12) <sup>d</sup>	E1
1570.2	3043.4	$(17/2^-) \rightarrow 15/2^+$	1.1(1)		(E1)
1721.2	2554.9	$(15/2^-) \rightarrow 13/2^+$	1.8(2)		(E1)
1748.2	3221.4	$(17/2^-) \rightarrow (15/2^+)$	0.20(2)		(E1)

continued...



TABLE I: continued...

$E_\gamma$	$E_x$	$J_i^\pi \rightarrow J_f^\pi$	$I_\gamma$ [1][2]	$R_{int}$	Multipolarity

---

[1] The quoted errors on intensities encompass errors due to background subtraction, fitting, and efficiency correction.

[2]  $W$  indicates weak transitions whose intensity could not be computed.

[3] <sup>a</sup>  $R_{int}$  obtained from gate on stretched quadrupole transition.

[4] <sup>d</sup>  $R_{int}$  obtained from gate on stretched dipole transition.

TABLE II: Measured level lifetimes and the corresponding B(M1) and B(E2) rates in  $^{103}\text{Ag}$ . The quoted uncertainties include the fitting errors and errors in side-feeding intensities

Band	$E_x$ (keV)	$\tau$ (ps)	$J^\pi$	B(M1) ( $\mu_N^2$ )	B(E2) ( $eb$ ) <sup>2</sup>
Band B	4941.6	$0.401^{+.11}_{-.06}$	$(29/2)^-$	$1.02^{+.30}_{-.20}$	$0.09^{+.02}_{-.03}$
	5300.9	$0.385^{+.04}_{-.06}$	$(31/2)^-$	$0.986^{+.10}_{-.20}$	$0.12^{+.01}_{-.01}$
	6167.7	$0.330^{+.04}_{-.03}$	$(33/2)^-$	$0.51^{+.06}_{-.06}$	$0.05^{+.005}_{-.005}$
Band C	5157.0	$0.390^{+.03}_{-.07}$	$(29/2)^-$	$2.6^{+.60}_{-.20}$	$0.09^{+.04}_{-.01}$
	5591.0	$0.32^{+.02}_{-.03}$	$(31/2)^-$	$2.2^{+.20}_{+.20}$	
	6133.8	$0.19^{+.01}_{-.03}$	$(33/2)^-$	$1.9^{+.30}_{-.20}$	
Band A	6166.7	$0.18^{+.02}_{-.02}$	$(31/2)^-$	$4.70^{+.50}_{+.50}$	
	6654.0	$0.13^{+.01}_{-.01}$	$(33/2)^-$	$3.72^{+.40}_{-.40}$	
	7157.8	$0.12^{+.01}_{-.01}$	$(35/2)^-$	$3.66^{+.35}_{-.35}$	

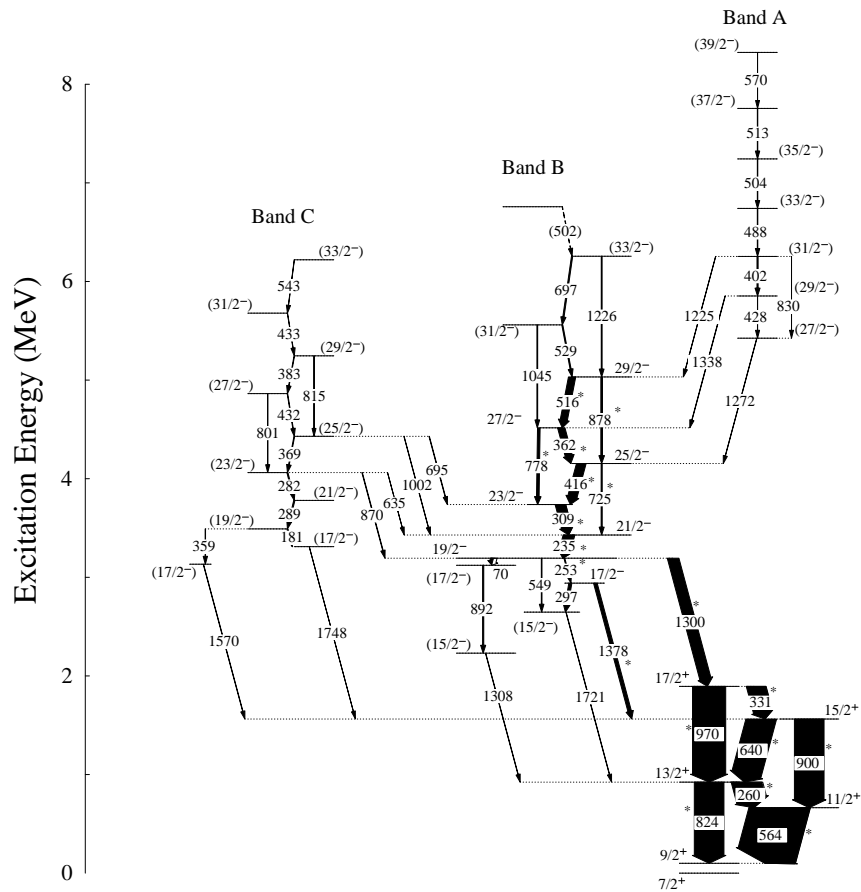


FIG. 1: Partial level scheme for  $^{103}\text{Ag}$  for the levels obtained from the  $^{72}\text{Ge}(^{35}\text{Cl}, 2p2n)^{103}\text{Ag}$  reaction. Previously-known transitions are marked with a (\*). The widths of the arrows are roughly proportional to the corresponding intensities. The spin and parity assignments given in parentheses are tentative.

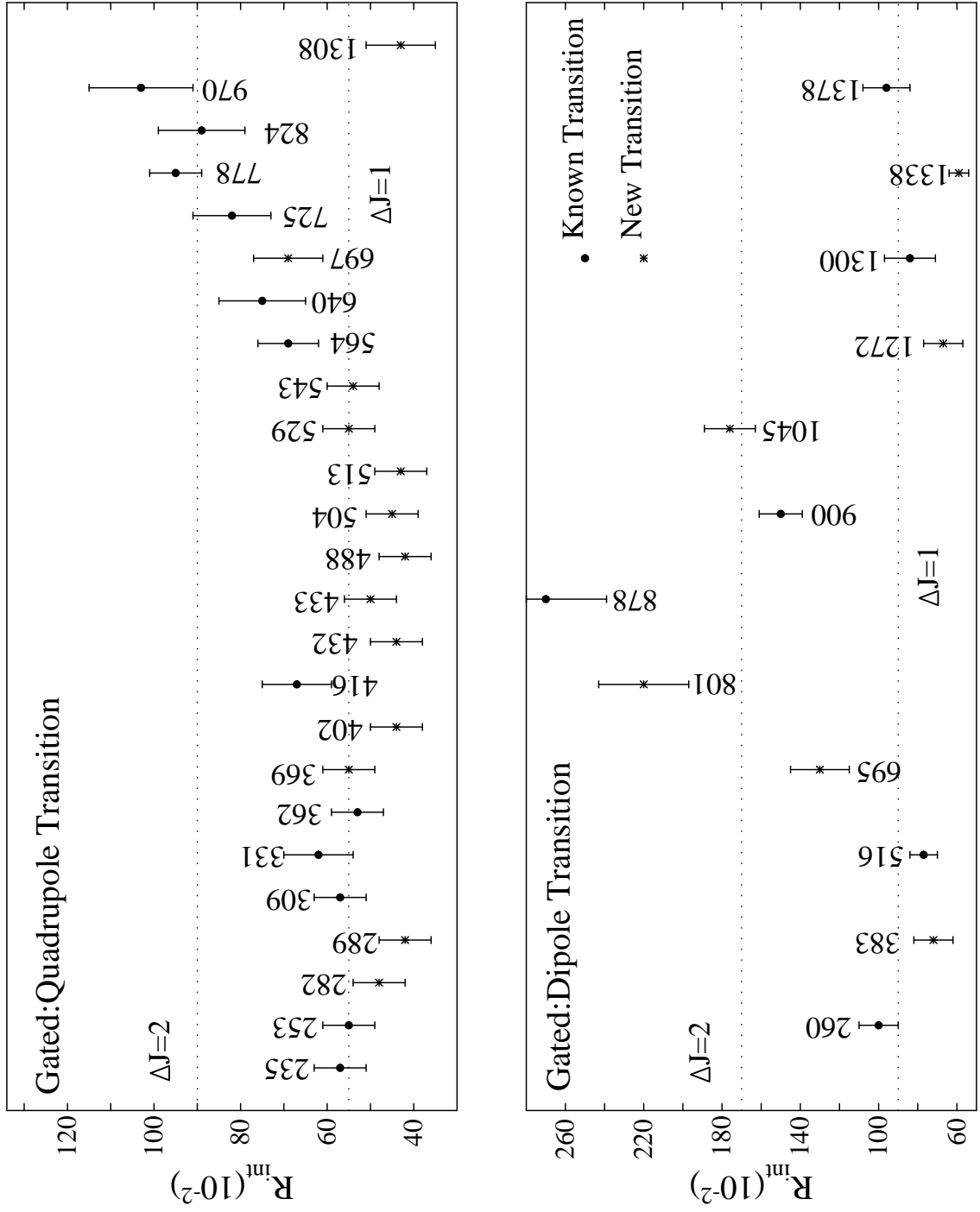


FIG. 2:  $R_{int}$  plotted for  $\gamma$ -ray transitions of  $^{103}\text{Ag}$ , using quadrupole transition and dipole transition as gates. The lines correspond to the value of  $R_{int}$  for the known quadrupoles and dipoles.

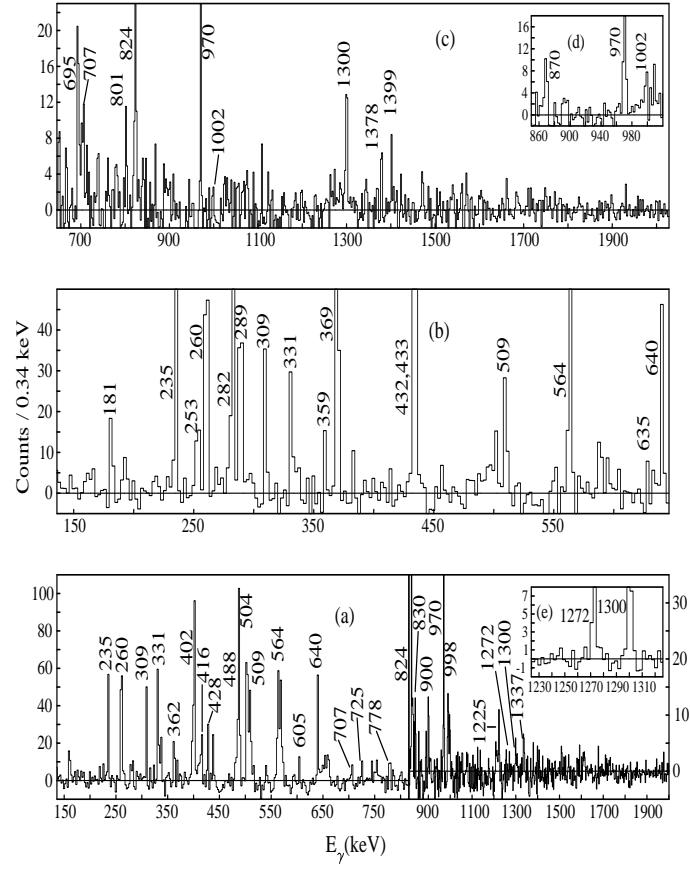


FIG. 3: Background subtracted  $\gamma$ - $\gamma$ - $\gamma$  spectra in  $^{103}\text{Ag}$  with double gates set on the 383- and 543-keV transitions of Band C (top and middle panel), and the 570- and 513-keV transitions of Band A (lower panel). The spectrum in inset (d) has been obtained from triple gates on 433-, 383- and 824-keV, transitions and the inset (e) from triple gates on the 402-, 428- and 235-keV transitions. The “linking” transitions for both bands are also indicated in the triple-gated spectra.

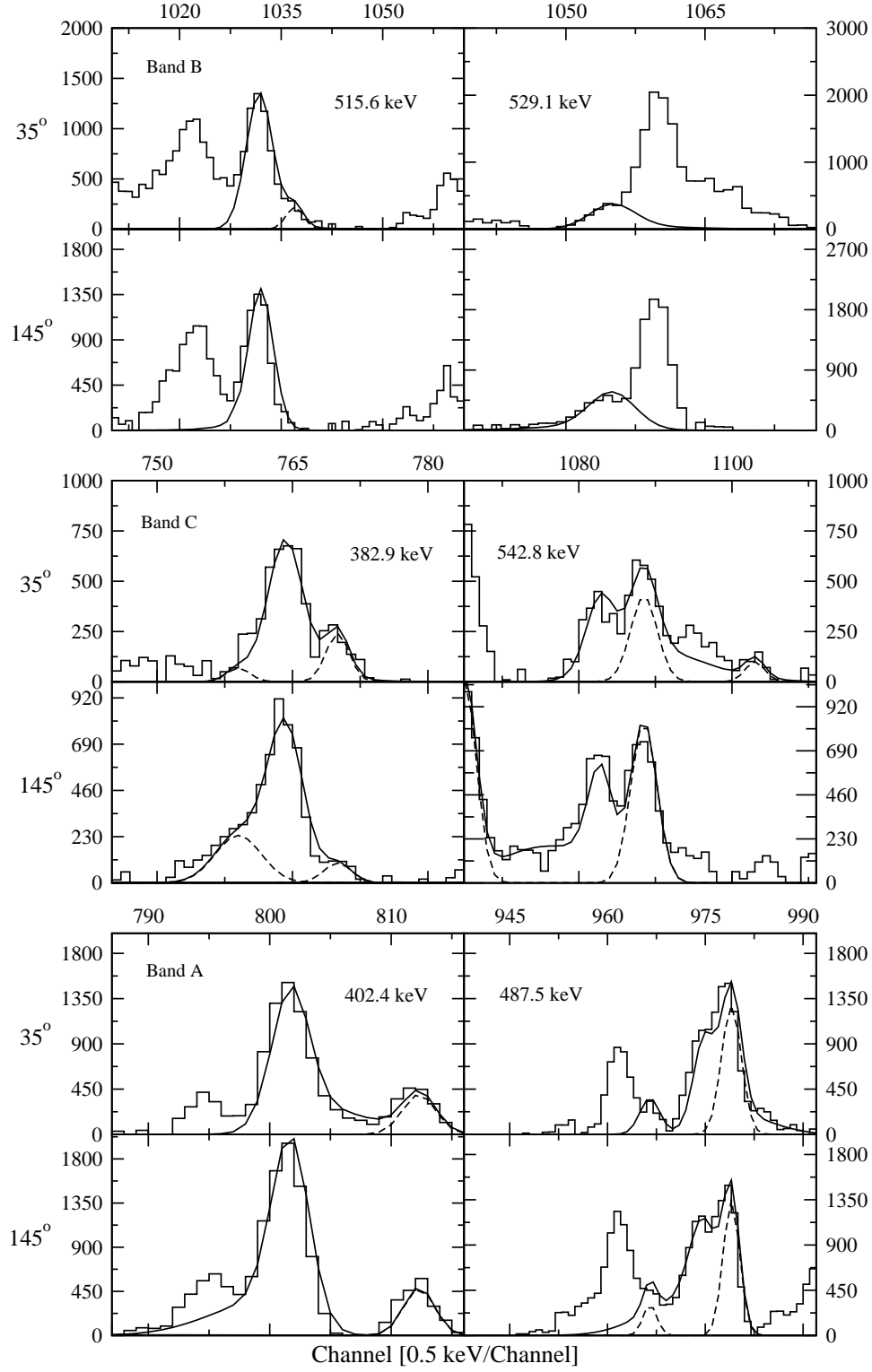


FIG. 4: Experimental and theoretical lineshapes for 383, 402, 488, 516, 529, and 543 keV  $\gamma$ - rays at the forward ( $35^\circ$ ; left panels) and backward ( $145^\circ$ ; right panels) angles with respect to the beam direction. Contaminant peaks are shown by dotted lines and theoretical line shape in solid lines.

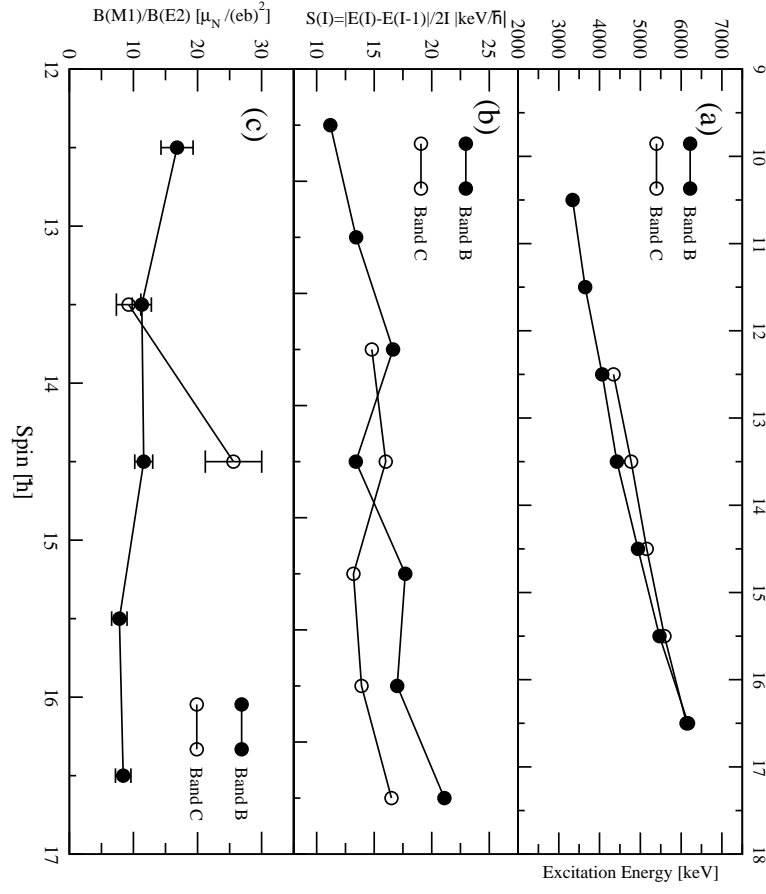


FIG. 5: Chiral fingerprints for Bands B and C in  $^{103}\text{Ag}$ : (a) excitation energy vs spin; (b)  $S(I)$  vs spin; (c)  $B(M1)/B(E2)$ .

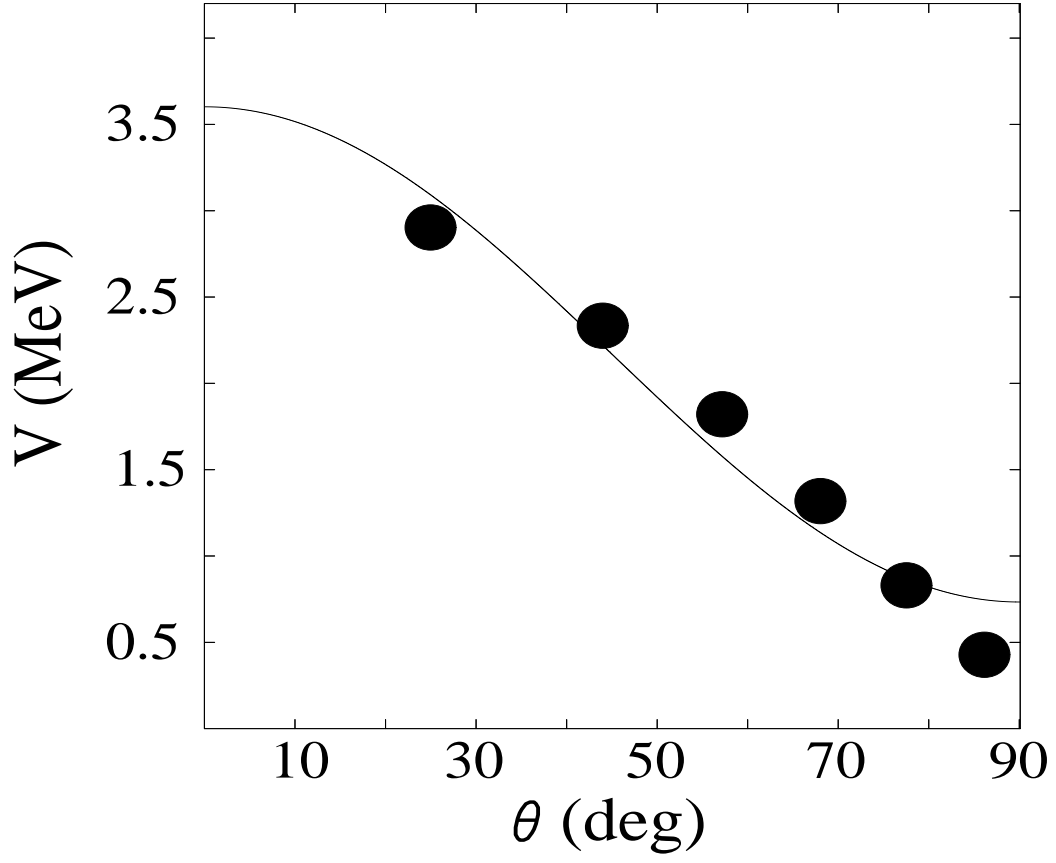


FIG. 6: The effective interaction between angular momentum vectors  $j_\pi$  and  $j_\nu$ , as a function of shears angle  $\theta$ . The solid curve is the expected dependence of a pure  $P_2$  term in the interaction, for Band A.



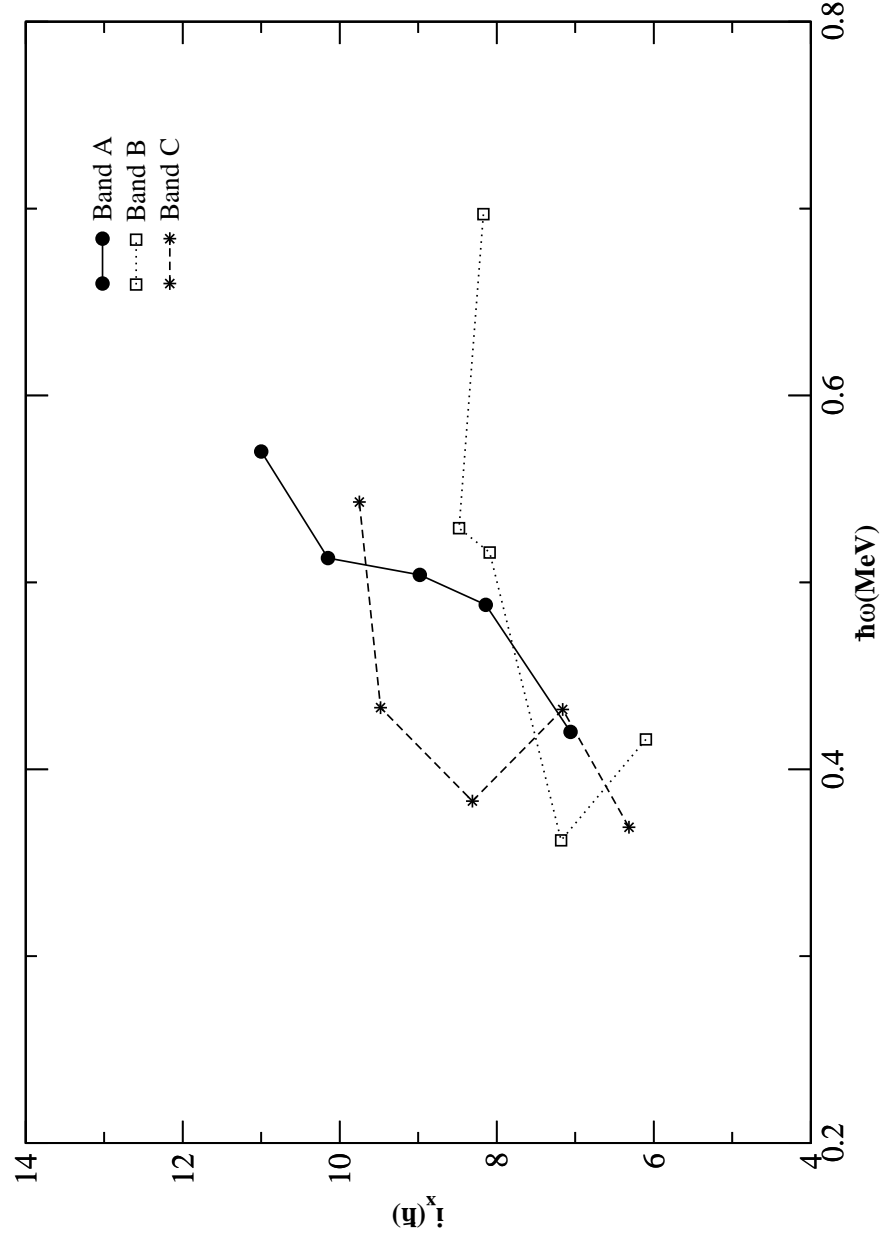


FIG. 7: Aligned angular momentum as a function of rotational frequency for Bands A, B, C. The experimental frequency is extracted from the measured  $\gamma$  energies using the relation  $\hbar\omega(I) = E_\gamma = E(I) - E(I - 1)$ . The reference parameters used are:  $\mathfrak{S}_0 = 7.0\hbar^2/\text{MeV}$  and  $\mathfrak{S}_1 = 15.0\hbar^4/\text{MeV}^3$

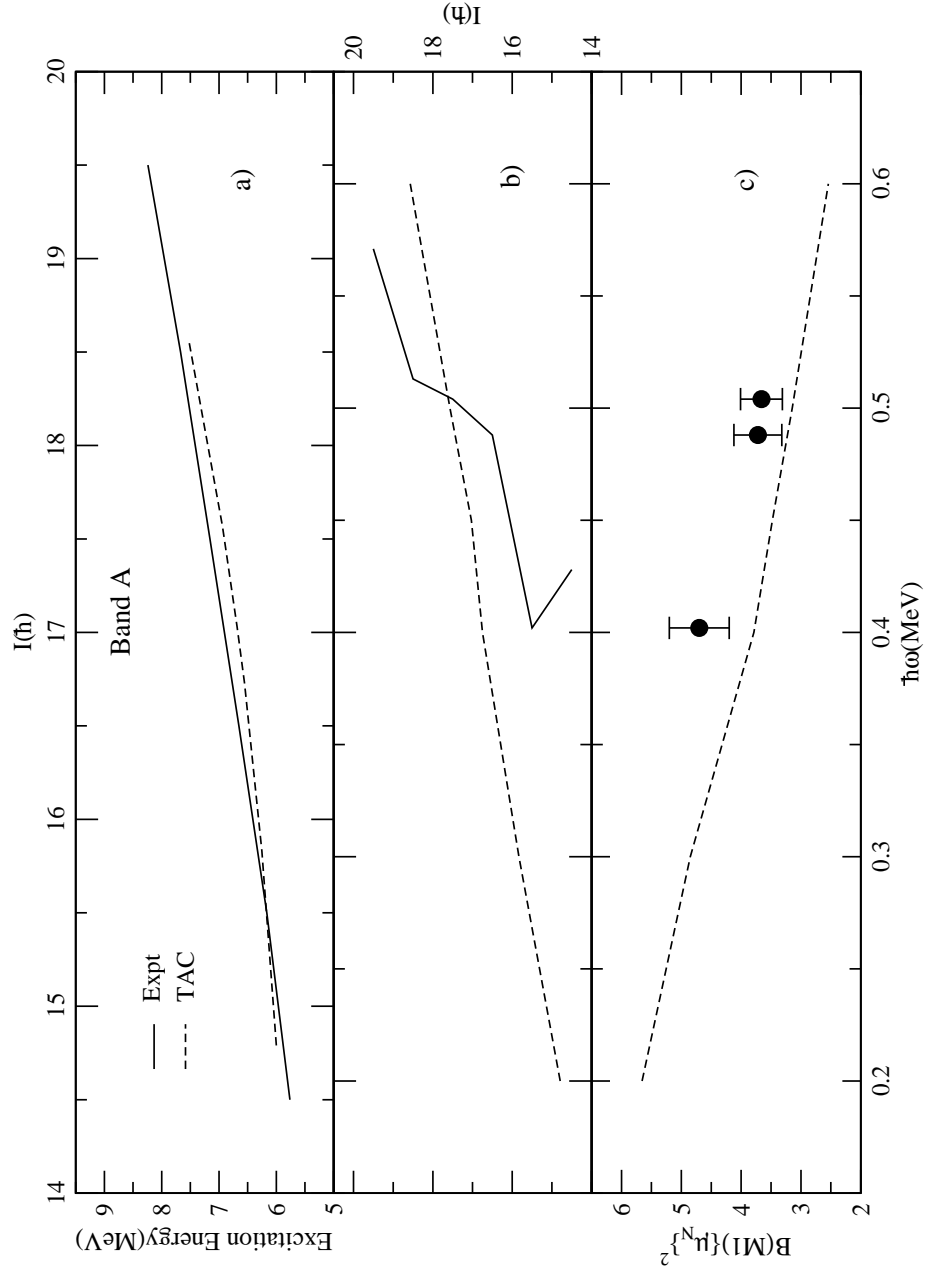


FIG. 8: (a) Excitation energy as a function of angular momentum; (b) Angular momentum and (c)  $B(M1)$  transition rates as a function of rotational frequency for Band A. The dashed line in (a), (b) and (c) are results of TAC calculation for the assigned configuration of Band A.

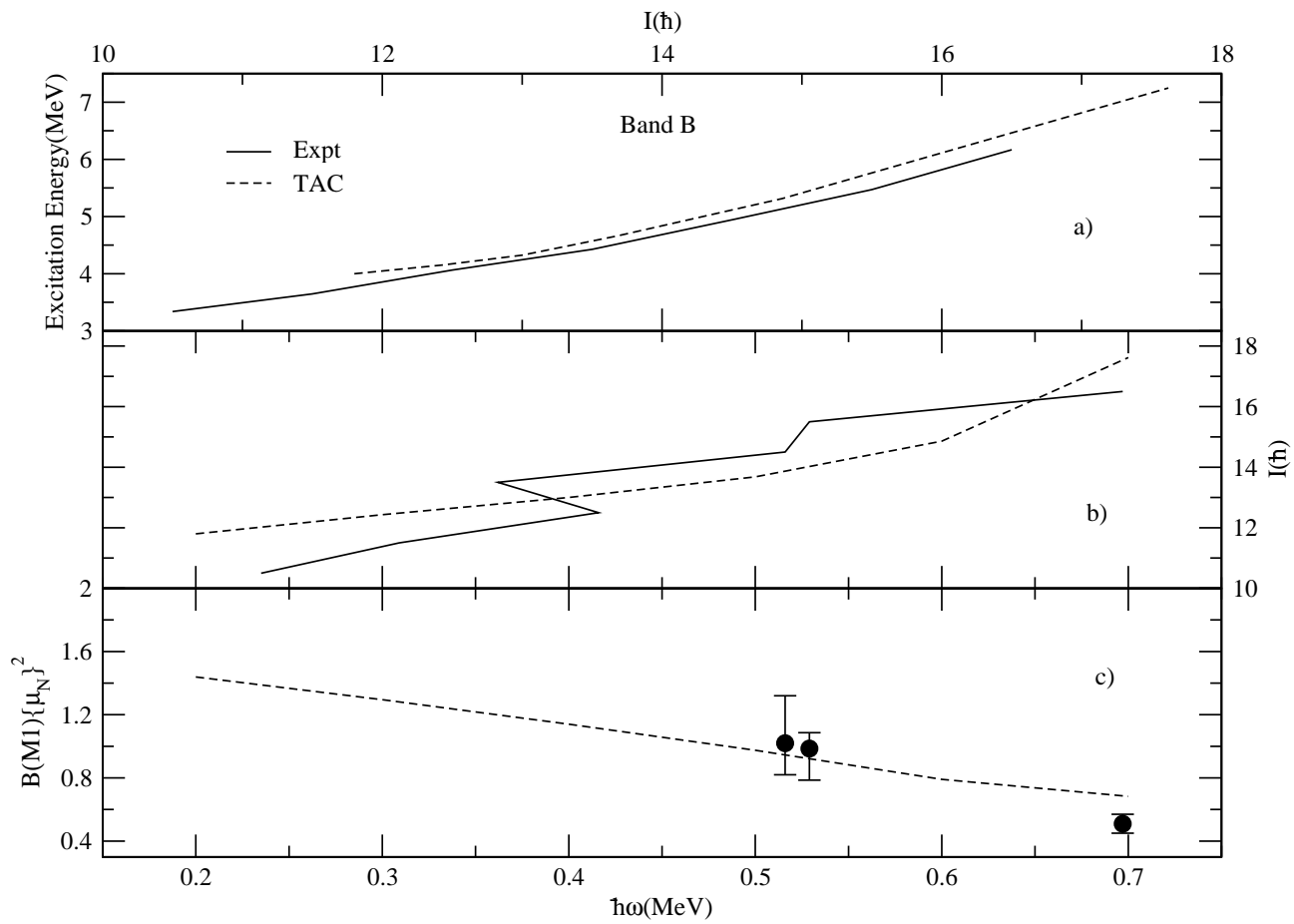


FIG. 9: Same as Fig. 8, but for Band B.

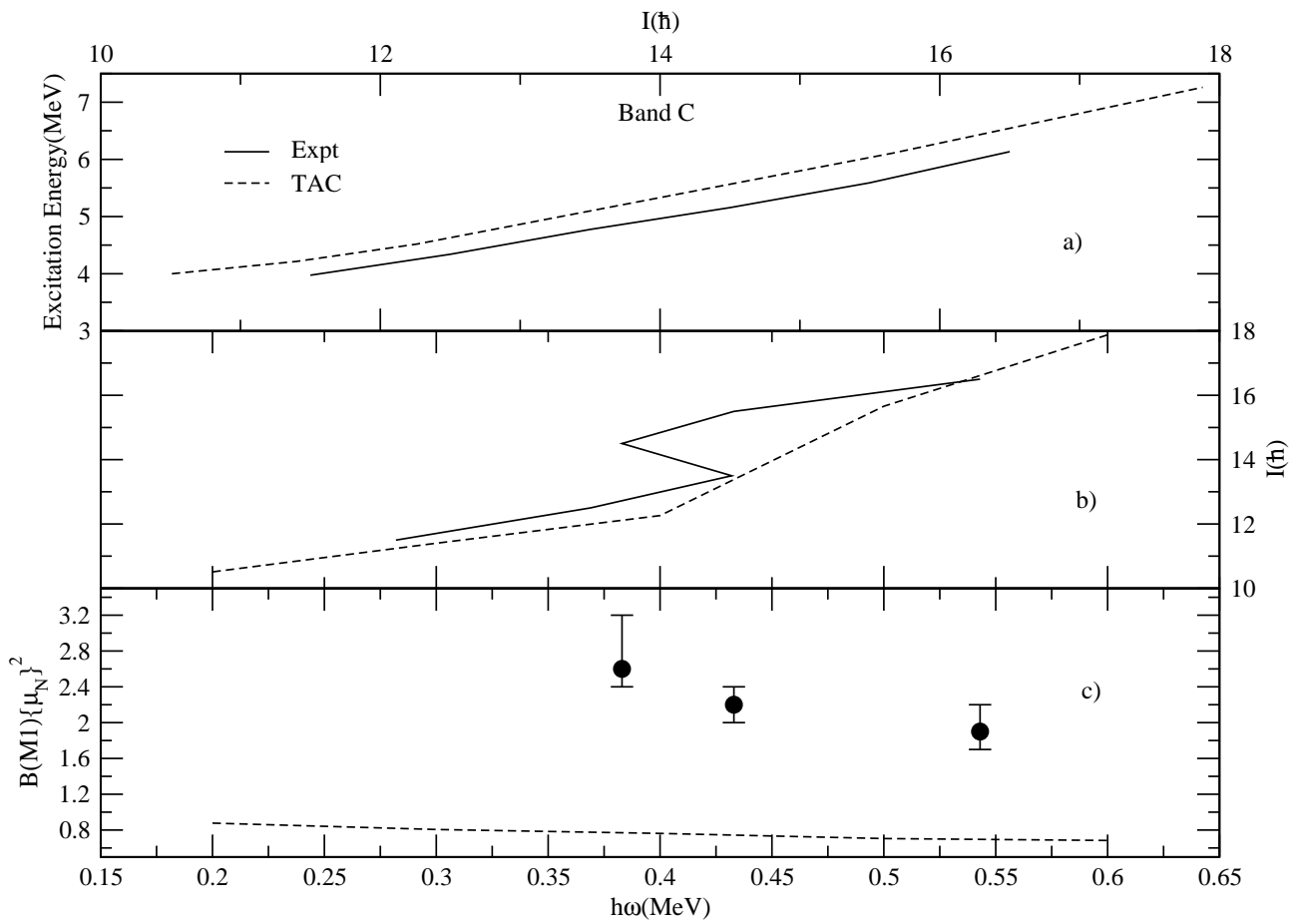


FIG. 10: Same as Fig. 8, but for Band C.